

1 Creating Artificial Human Genomes Using Generative 2 Models

3
4 **Authors:** Burak Yelmen^{1,2,*}, Aurélien Decelle³, Linda Ongaro^{1,2}, Davide Marnetto¹, Corentin
5 Tallec³, Francesco Montinaro^{1,4}, Cyril Furtlehnner³, Luca Pagani^{1,5}, Flora Jay^{3,*}

6
7 **Affiliations:**

8 1 *Institute of Genomics, University of Tartu, Estonia*

9 2 *Institute of Molecular and Cell Biology, University of Tartu, Estonia*

10 3 *Laboratoire de Recherche en Informatique, CNRS UMR 8623, Université Paris-Sud,*

11 *Université Paris-Saclay, Orsay, France*

12 4 *Department of Zoology, University of Oxford, UK*

13 5 *APE Lab, Department of Biology, University of Padova, Italy*

14 *to whom correspondence should be addressed: burakyelmen@gmail.com, flora.jay@iri.fr

15 Abstract

16 Generative models have shown breakthroughs in a wide spectrum of domains due to
17 recent advancements in machine learning algorithms and increased computational
18 power. Despite these impressive achievements, the ability of generative models to
19 create realistic synthetic data is still under-exploited in genetics and absent from
20 population genetics.

21

22 Yet a known limitation of this field is the reduced access to many genetic databases
23 due to concerns about violations of individual privacy, although they would provide a
24 rich resource for data mining and integration towards advancing genetic studies. In this
25 study, we demonstrated that deep generative adversarial networks (GANs) and
26 restricted Boltzmann machines (RBMs) can be trained to learn the high dimensional
27 distributions of real genomic datasets and create high quality artificial genomes (AGs)
28 with none to little privacy loss. To illustrate the promising outcomes of our method, we
29 showed that (i) imputation quality for low frequency alleles can be improved by
30 augmenting reference panels with AGs, (ii) scores obtained from selection tests on
31 AGs and real genomes are highly correlated and (iii) AGs can inherit genotype-
32 phenotype associations. AGs have the potential to become valuable assets in genetic
33 studies by providing high quality anonymous substitutes for private databases.

34

35 **Introduction**

36 Availability of genetic data has increased tremendously due to advances in sequencing
37 technologies and reduced costs (Mardis 2017). The vast amount of human genetic
38 data is used in a wide range of fields, from medicine to evolution. Despite the
39 advances, cost is still a limiting factor and more data is always welcomed, especially
40 in population genetics and genome-wide association studies (GWAS) which usually
41 require substantial amounts of samples. Partially related to the costs but also to the
42 research bias toward studying populations of European ancestry, many autochthonous
43 populations are under-represented in genetic databases, diminishing the extent of the
44 resolution in many studies (Cann 2002; Popejoy and Fullerton 2016; Mallick et al.
45 2016; Sirugo et al. 2019). Additionally, a huge portion of the data held by government
46 institutions and private companies is considered sensitive and not easily accessible
47 due to privacy issues, exhibiting yet another barrier for scientific work. A class of
48 machine learning methods called generative models might provide a suitable solution
49 to these problems.

50

51 Generative models are used in unsupervised machine learning to discover intrinsic
52 properties of data and produce new data points based on those. In the last decade,
53 generative models have been studied and applied in many domains of machine
54 learning (Libbrecht and Noble 2015; Zhang et al. 2017; Rolnick and Dyer 2019). There
55 have also been a few applications in the genetics field (Davidsen et al. 2019; Liu et al.
56 2019; Tubiana et al. 2019; Shimagaki and Weigt 2019), one specific study focusing on
57 generating DNA sequences via deep generative models to capture protein binding
58 properties (Killoran et al. 2017). Among the various generative approaches, we focus
59 on two of them in this study, generative adversarial networks (GANs) and restricted
60 Boltzmann machines (RBMs). GANs are generative neural networks which are
61 capable of learning complex data distributions in a variety of domains (Goodfellow et
62 al. 2014). A GAN consists of two neural networks, a generator and a discriminator,
63 which compete in a zero-sum game (Supplementary Figure 1). During training, the
64 generator produces new instances while the discriminator evaluates their authenticity.
65 The training objective consists in learning the data distribution in a way such that the
66 new instances created by the generator cannot be distinguished from true data by the
67 discriminator. Since their first introduction, there have been several successful

68 applications of GANs, ranging from generating high quality realistic imagery to gap
69 filling in texts (Ledig et al. 2017; Fedus et al. 2018). GANs are currently the state-of-
70 the-art models for generating realistic images (Brock et al. 2018).

71

72 A restricted Boltzmann machine, initially called Harmonium is another generative
73 model which is a type of neural network capable of learning probability distributions
74 through input data (Smolensky 1986; Teh and Hinton 2001). RBMs are two layer neural
75 networks consisting of an input (visible) layer and a hidden layer (Supplementary
76 Figure 2). The learning procedure for the RBM consists in maximizing the likelihood
77 function over the visible variables of the model. This procedure is done by adjusting
78 the weights such that the correlations between the visible and hidden variables on both
79 the dataset and sampled configurations from the RBM converge. Then RBM models
80 recreate data in an unsupervised manner through many forward and backward passes
81 between these two layers (Gibbs sampling), corresponding to sampling from the
82 learned distribution. The output of the hidden layer goes through an activation function,
83 which in return becomes the input for the hidden layer. Although mostly overshadowed
84 by recently introduced approaches such as GANs or Variational Autoencoders
85 (Kingma and Welling 2013), RBMs have been used effectively for different tasks (such
86 as collaborative filtering for recommender systems, image or document classification)
87 and are the main components of deep belief networks (Hinton and Salakhutdinov 2006;
88 Hinton 2007; Larochelle and Bengio 2008).

89

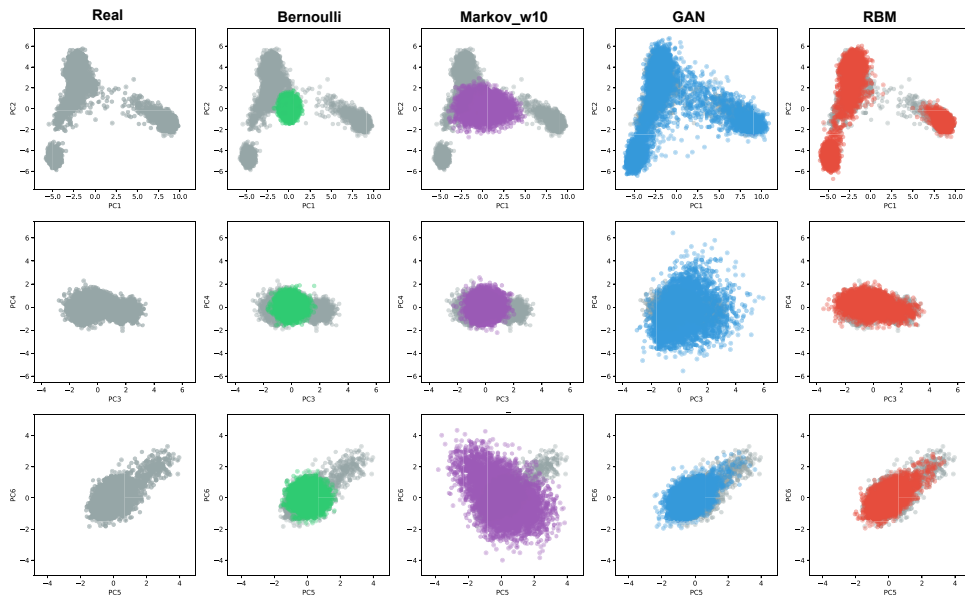
90 Here we propose and compare a prototype GAN model along with an RBM model to
91 create Artificial Genomes (AGs) which can mimic real genomes and capture population
92 structure along with other characteristics of real genomes. We envision two main
93 applications of our generative methods: (i) improving the performance of genomic
94 tasks such as imputation, ancestry reconstruction, GWAS studies, by augmenting
95 genomic panels with AGs serving as proxies for private datasets, (ii) demonstrating
96 that a proper encoding of the genomic data can be learned and possibly used as a
97 starting input of various inference tasks by combining this encoding with recent neural
98 network-based tools for the reconstruction of recombination, demography or selection
99 (Sheehan and Song 2016; Adrion et al. 2019; Flagel et al. 2019).

100 **Results**

101 **Reconstructing genome wide population structure:**

102 Initially we created AGs with GAN, RBM, and two simple generative models for
103 comparison: a Bernoulli and a Markov chain model (see Materials & Methods) using
104 2504 individuals (5008 haplotypes) from 1000 Genomes data (1000 Genomes Project
105 Consortium et al. 2015), spanning 805 SNPs from all chromosomes which reflect a
106 high proportion of the population structure present in the whole dataset (Colonna et al.
107 2014). Both GAN and RBM models capture a good portion of the population structure
108 present in 1000 Genomes data while the other two models could only produce
109 instances centered around 0 on principal component analysis (PCA) space (Figure 1).
110 All major modes, corresponding to African, European and Asian genomes, are well
111 represented in AGs produced by GAN and RBM models. Uniform manifold
112 approximation and projection (UMAP) mapping results also correlate with the
113 performed PCA (Supplementary Figure 3). We additionally checked the distribution of
114 pairwise differences of haploid genomes to see how different AGs are from real
115 genomes (Supplementary Figure 4). Both RBM and GAN models have highly similar
116 distributions to the distribution of pairwise differences of the real genomes within
117 themselves. Especially RBM excels at replicating the real peaks, indicating a high
118 similarity with real genomes. Since GANs and RBMs showed an excellent performance
119 for this use case, we further explored other characteristics using only these two
120 models.

121 **Figure 1.** The six first axes of a PCA applied to real (gray) and artificial genomes (AGs)
122 generated via Bernoulli (green), Markov chain (purple), GAN (blue) and RBM (red)
123 models. There are 5000 haplotypes for each AG dataset and 5008 (2504 genomes)
124 for the real dataset from 1000 Genomes spanning 805 informative SNPs. See
125 Materials & Methods for detailed explanation of the generation procedures.



126
127
128 Furthermore, similarly to tSNE and UMAP, RBMs perform a non-linear dimension
129 reduction of the data and provides a suitable representation of a genomic dataset as
130 a by-product based on the non-linear feature space associated to the hidden layer
131 (Supplementary Text). As Diaz-Papkovich et al (Diaz-Papkovich et al. 2019), we found
132 that the RBM representation differs from the linear PCA ones. Here we plot the
133 representation corresponding to the selected RBM model and exhibit its rapid evolution
134 through training (Supplementary Figure 5).

135
136 Supplementary Figure 5 shows that African, East Asian, and to a lesser extent,
137 European populations stand out on the two first components. The Finnish are slightly
138 isolated from the other European (similar to Peruvian from American) populations on
139 the first two components. South Asians are located at the center separated from
140 Europeans, partially overlapping with American populations, and stand out at
141 dimension 5 and higher. Interestingly when screening the hidden node activations, we
142 observed that different populations or groups activate different hidden nodes, each one

143 representing a specific combination of SNPs, thereby confirming that the hidden layer
144 provides a meaningful encoding of the data (Supplementary Figure 6).

145

146 **Reconstructing local high-density haplotype structure:**

147 To evaluate if high quality artificial dense genome sequences can also be created by
148 generative models, we applied the GAN and RBM methods to a 10K SNP region using
149 (i) the same individuals from 1000 Genomes data and (ii) 1000 Estonian individuals
150 from the high coverage Estonian Biobank (Leitsalu et al. 2015) to generate artificial
151 genomes. PCA results of AGs spanning consecutive 10K SNPs show that both GAN
152 and RBM models can still capture the relatively toned-down population structure
153 (Supplementary Figure 7) as well as the overall distribution of pairwise distances
154 (Supplementary Figure 8). Looking at the allele frequency comparison between real
155 and artificial genomes, we see that especially GAN performs poorly for low frequency
156 alleles, due to a lack of representation of these alleles in the AGs (Supplementary
157 Figure 9). On the other hand, the distribution of the distance of real genomes to the
158 closest AG neighbour shows that GAN model, although slightly underfitting,
159 outperforms RBM model, for which an excess of small distances points towards slight
160 overfitting (Supplementary Figure 10).

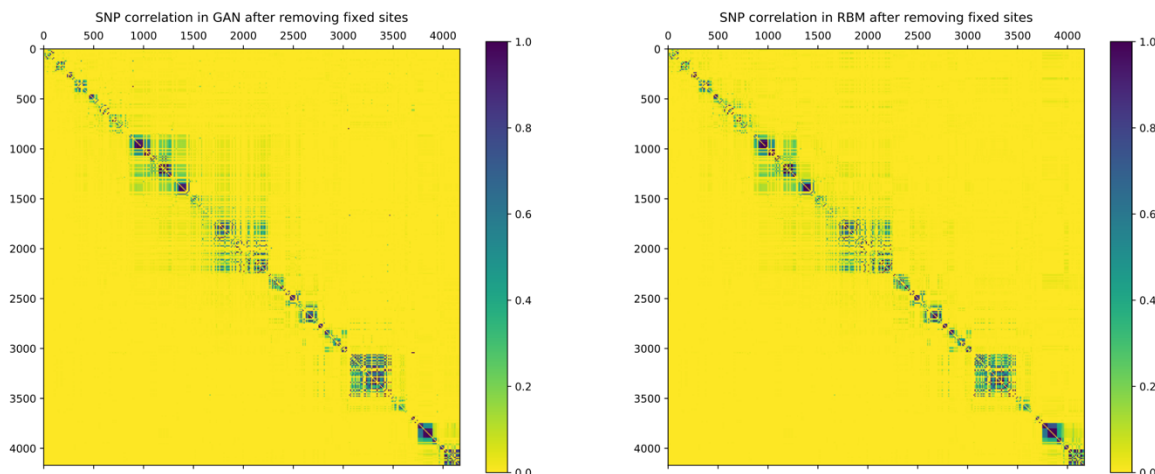
161

162 Additionally, we performed linkage disequilibrium (LD) analyses comparing artificial
163 and real genomes to assess how successfully the AGs imitate short and long range
164 correlations between SNPs. Pairwise LD matrices for real and artificial genomes all
165 show a similar block pattern demonstrating that GAN and RBM accurately captured
166 the overall structure with SNPs having higher linkage in specific regions (Figure 2a).
167 However, plotting LD as a function of the SNP distance showed that all models capture
168 weaker correlation, with RBM outperforming the GAN model perhaps due to its slightly
169 overfitting characteristic (Figure 2b). To further determine the haplotypic integrity of
170 AGs, we performed ChromoPainter (Lawson et al. 2012) and Haplostrips (Marnetto
171 and Huerta-Sánchez 2017) analyses on AGs created using Estonians as the training
172 data. It was visually impossible to distinguish the difference between real and artificial
173 genomes in terms of local haplotypic structure with Haplostrips (Supplementary Figure
174 11). However, majority of the AGs produced via GAN model displayed an excess of
175 short chunks when painted against 1000 Genomes individuals, whereas RBM AGs
176 were nearly indistinguishable from real genomes (Supplementary Figure 12).

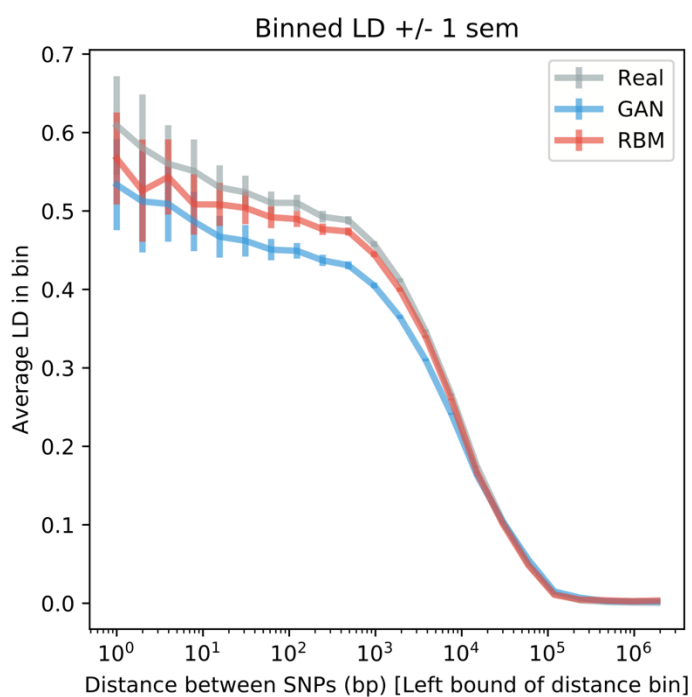
177 **Figure 2. Linkage disequilibrium (LD) analysis on real and artificial Estonian genomes.**
178 **a)** Correlation (r^2) matrices of SNPs. Lower triangular parts are SNP pairwise
179 correlation in real genomes and upper triangular parts are SNP pairwise correlation in
180 artificial genomes. **b)** LD as a function of SNP distance. Pairwise SNP distances were
181 stratified into 50 bins and for each distance bin, the correlation was averaged over all
182 pairs of SNPs belonging to the bin.

183

a.



b.



184
185

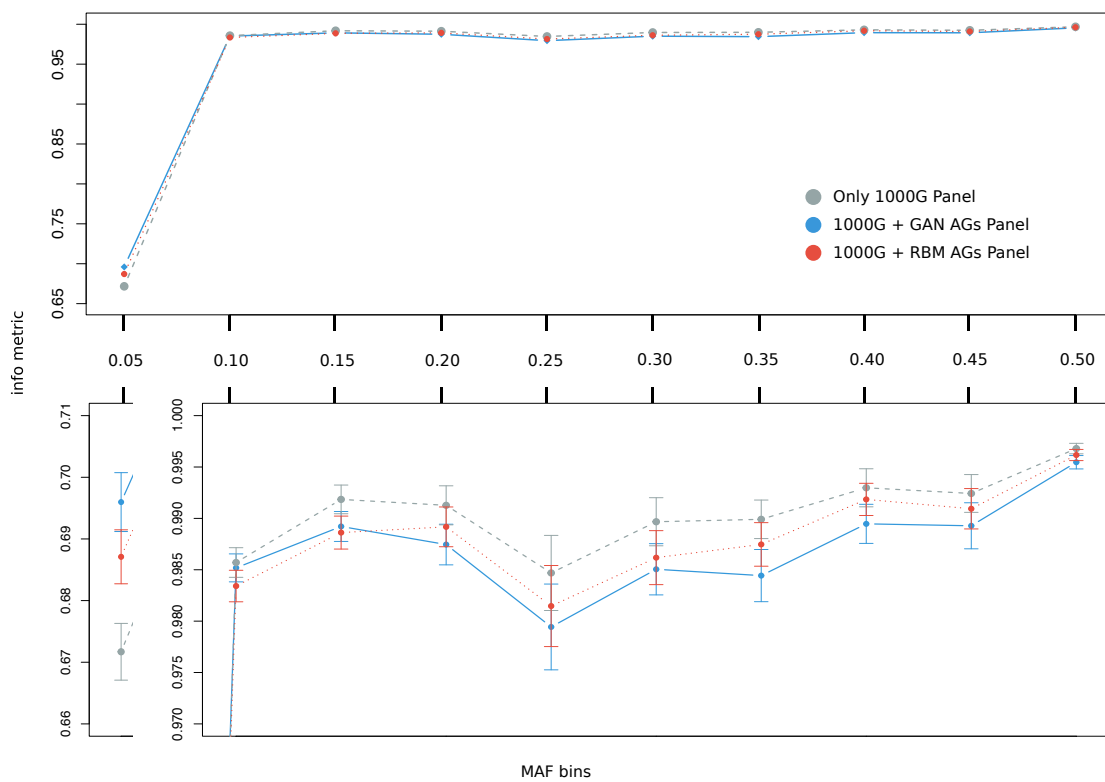
186 After demonstrating that our models generated realistic AGs according to the
187 described summary statistics, we investigated further whether they respected privacy
188 by measuring the extent of overfitting. We calculated two metrics of resemblance and
189 privacy, the nearest neighbour adversarial accuracy (AA_{TS}) and privacy loss presented
190 in a recent study (Yale et al. 2019). AA_{TS} score measures whether two datasets were
191 generated by the same distribution based on the distances between all data points and
192 their nearest neighbours in each set. When applied to artificial and real datasets, a
193 score between 0.5 and 1 indicates underfitting, between 0 and 0.5 overfitting (and likely
194 privacy loss), and exactly 0.5 indicates that the datasets are indistinguishable. By using
195 an additional real test set, it is also possible to calculate a privacy loss score that is
196 positive in case of information leakage, negative otherwise, and approximately ranges
197 from -0.5 to 0.5. Computed on our generated data, both scores support haplotypic
198 pairwise difference results confirming the underfitting nature of GAN AGs and slightly
199 overfitting nature of RBM AGs with a small risk of privacy leakage for the latter
200 (Supplementary Figure 13).

201

202 Since it has been shown in previous studies that imputation scores can be improved
203 using additional population specific reference panels (Gurdasani et al. 2015; Mitt et al.
204 2017), as a possible future use case, we tried imputing real Estonian genomes using
205 1000 Genomes reference panel and additional artificial reference panels with Impute2
206 software (Howie et al. 2011). Both combined RBM AG and combined GAN AG panels
207 outperformed 1000 Genomes panel for the lowest MAF bin (for $MAF < 0.05, 0.015$ and
208 0.024 improvement respectively) which had 5926 SNPs out of 9230 total (Figure 3).
209 Also mean info metric over all SNPs was 0.009 and 0.015 higher for combined RBM
210 and GAN panels respectively, compared to the panel with only 1000 Genomes
211 samples. However, aside from the lowest MAF bin, 1000 Genomes panel
212 outperformed both concatenated panels for all the higher bins. This might be a
213 manifestation of haplotypic deformities in AGs that might have disrupted the imputation
214 algorithm.

215

216 **Figure 3.** Imputation evaluation of three different reference panels based on Impute2
217 software's info metric. Imputation was performed on 8678 Estonian individuals (which
218 were not used in training of GAN and RBM models) using only 1000 Genomes panel
219 (gray), combined 1000 Genomes and GAN artificial genomes panel (blue) and
220 combined 1000 Genomes and RBM artificial genomes panel (red). SNPs were divided
221 into 10 MAF bins, from 0.05 to 0.5, after which mean info metric values were calculated.
222 Bars in the zoomed section show the standard error of mean.

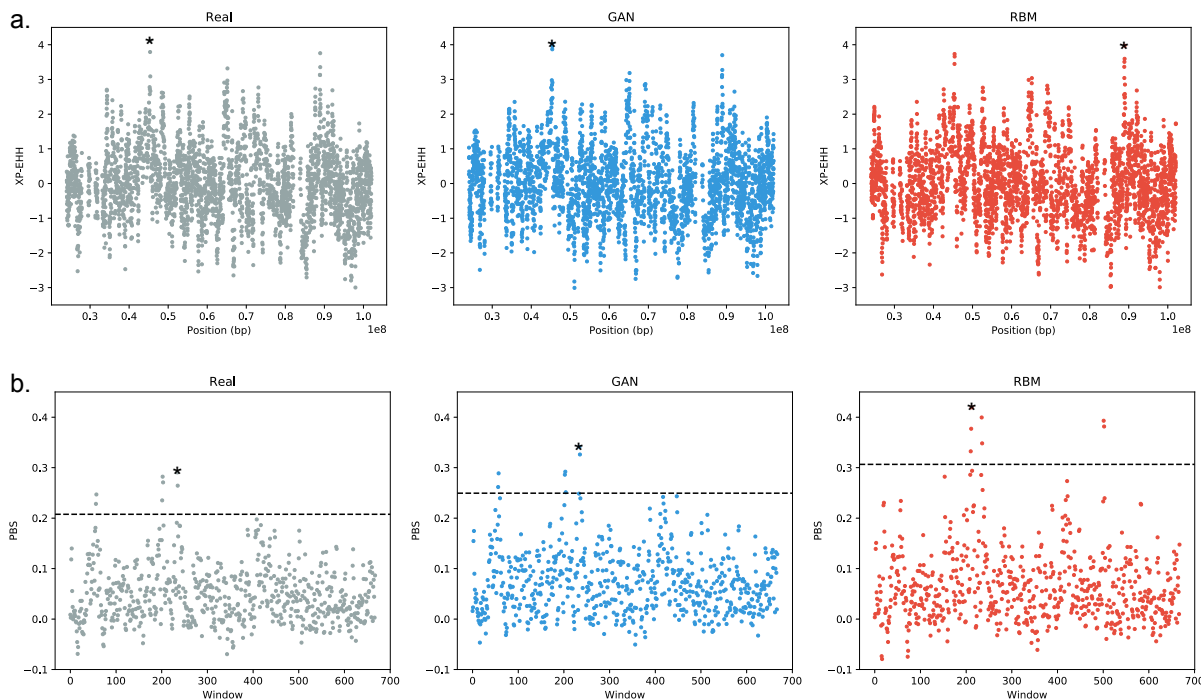


223
224
225 **Selection tests:**
226 We additionally performed cross population extended haplotype homozygosity (XP-
227 EHH) and population branch statistic (PBS) on a 3348 SNP region homogenously
228 dispersed over chromosome 15 to assess if AGs can also be used for selection tests.
229 Both XP-EHH and PBS results provided high correlation between the scores of real
230 and artificial genomes (Figure 4). The peaks observed in real genome scores which
231 might indicate possible selection signals were successfully captured by AGs.
232

233 **Figure 4.** Selection tests on chromosome 15. **a)** Standardized XP-EHH scores of real
234 and artificial Estonian genomes using 1000 Genomes Yoruba population (YRI) as the

235 complementary population. Correlation coefficient between real and GAN XP-EHH
236 score is 0.902, between real and RBM XP-EHH score is 0.887. **b)** PBS scores of real
237 and artificial Estonian genomes using 1000 Genomes Yoruba (YRI) and Japanese
238 (JPT) populations as the complementary populations. PBS window size is 10 and step
239 size is 5. Dotted black line corresponds to the 99th percentile. Correlation coefficient
240 between real and GAN PBS score is 0.923, between real and RBM PBS score is 0.755.
241 Highest peaks are marked by an asterisk.

242



243

244

245

246 **Linking genotypes with phenotypes:**

247 We then explored the possibility of creating AGs with unphased genotype data and
248 recreating phenotype-genotype associations using generative models. As a proof of
249 concept, we created GAN AGs via training on 1925 Estonian individuals with 5000
250 SNPs using unphased genotypes instead of haplotypes. There was an additional
251 column in this dataset representing eye color (blue or brown). This region
252 encompasses rs12913832 SNP which is highly associated with eye color phenotype
253 (Han et al. 2008; Eriksson et al. 2010; Zhang et al. 2013). In our real genome dataset,
254 nearly 96% of the individuals possessing at least one ancestral allele (A) have brown
255 eye color while this percentage is 80% in GAN AGs. Similarly, 97% of all blue-eyed
256 real individuals and 88% of the artificial ones are homozygous for the derived allele

257 (G). No blue-eyed individuals are homozygous for the ancestral alleles in the real
258 dataset and only 9 individuals out of the 1925 GAN AGs were homozygous ancestral
259 with blue eyes (Supplementary Table). Chi-square tests based on the contingency
260 tables were highly significant for both the real and artificial datasets (p-values < 2.2e-
261 16 ; Supplementary Table 1). These results suggest that AGs were able to reproduce
262 the genotypic-phenotypic association existing in the real dataset. We could not detect
263 the same association in the RBM AG dataset (see Discussion).

264 Discussion

265 In this study, we applied generative models to produce artificial genomes and
266 evaluated their characteristics. To the best of our knowledge, this is the first application
267 of GAN and RBM models in population genetics context, displaying overall promising
268 applicability. We showed that population structure and frequency-based features of
269 real populations can successfully be preserved in AGs created using GAN and RBM
270 models. Furthermore, both models can be applied to sparse or dense SNP data given
271 a large enough number of training individuals. Our different trials showed that the
272 minimum required number of individuals for training is highly variable, possibly
273 correlated with the diversity among individuals (data not shown). Since haplotype data
274 is more informative, we created haplotypes for the analyses but we also demonstrated
275 that the GAN model can be applied to genotype data too, by simply combining two
276 haplotypes if the training data is not phased (see Materials & Methods). In addition, we
277 showed that it is possible to generate AGs with simple phenotypic traits through
278 genotype data (see Results). Even though there were only two simple classes, blue
279 and brown eye color phenotypes, generative models can be improved in the future to
280 hold the capability to produce artificial datasets combining AGs with multiple
281 phenotypes. The training of the RBM in this case did not work properly. We believe
282 that it is because the encoding of the phenotype is not well-suited for the RBM. Further
283 investigation on that part would be out of the scope of this article, but we suspect that
284 an encoding of the type "one-hot" vector addition of a stronger learning rate for the
285 weights linked to the phenotype nodes could improve the training.

286

287 One major drawback of the proposed models is that, due to computational limitations,
288 they cannot yet be harnessed to create whole artificial genomes but rather snippets or
289 sequential dense chunks. Although parallel computing might be a solution, this might
290 further disrupt the haplotype structure in AGs. Instead, adapting convolutional GANs
291 for AG generation might be a possible solution in the future (Radford et al. 2016).
292 Another problem arose due to rare alleles, especially for the GAN model. We showed
293 that nearly half of the alleles become fixed in the GAN AGs in the 10K SNP dataset,
294 whereas RBM AGs capture more of the rare alleles present in real genomes
295 (Supplementary Figure 14). A known issue in GAN training is mode collapse (Salimans
296 et al. 2016), which occurs when the generator fails to cover the full support of the data

297 distribution. This failure case could explain the inability of GANs to generate rare
298 alleles. For some applications relying on rare alleles, GAN models less sensitive to
299 mode dropping would be a promising alternative (Arjovsky et al. 2017; Lucas et al.
300 2018).

301

302 An important use case for the AGs in the future might be creating publicly available
303 versions of private genome banks. Through enhancements in scientific knowledge and
304 technology, genetic data becomes more and more sensitive in terms of privacy. AGs
305 might offer a versatile solution to this delicate issue in the future by protecting the
306 anonymity of real individuals. Our results showed that GAN AGs are possibly
307 underfitting while, on the contrary, RBM AGs are slightly overfitting, based on
308 distribution of minimum distance to the closest neighbour (Supplementary Figure 10)
309 and AA_{TS} scores (Supplementary Figure 13a), although we showed how overfitting
310 could be restrained by integrating AA_{TS} scores within our models as a criterion for early
311 stopping in training (before the networks start overfitting). In the context of the privacy
312 issue, GAN AGs have a slight advantage since underfitting is preferable. More distant
313 AGs would hypothetically be harder to be traced back to the original genomes. We
314 also tested the sensitivity of the AA_{TS} score and privacy loss (Supplementary Figure
315 15). It appears that both scores are affected very slightly when we add only a few real
316 genomes to the AG dataset from the training set. Although this case is easily detectable
317 by examining the extreme left tail of the pairwise distribution, it advocates for combining
318 multiple privacy loss criteria and developing other sensitive measurement techniques
319 for better assessment of generated AGs. Additionally, even though we did not detect
320 exact copies of real genomes in AG sets created either by RBM or GAN models, it is
321 a very complicated task to determine if the generated samples can be traced back to
322 the originals. Reliable measurements need to be developed in the future to assure
323 complete anonymity of the source individuals given the released AGs. In particular, we
324 will investigate whether the differential privacy framework is performant in the context
325 of large population genomics datasets (Dwork et al. 2006; Torkzadehmahani et al.
326 2019).

327

328 Imputation results demonstrated promising outcomes especially for population specific
329 low frequency alleles. However, imputation with both RBM and GAN AGs integrated
330 reference panels showed slight decrease of info metric for higher frequency alleles

331 compared to only 1000 Genomes panel (Figure 3). We initially speculated that this
332 might be related to the disturbance in haplotypic structure and therefore, tried to filter
333 AGs based on chunk counts from ChromoPainter results, preserving only AGs which
334 are below the average chunk count of real genomes. The reasoning behind this was
335 to preserve most real-alike AGs with undisturbed chunks. Even with this filtering, slight
336 decrease in higher MAF bins was still present (data not shown). Yet results of
337 implementation with AGs for low frequency alleles and without AGs for high frequency
338 ones could be combined to achieve best performance. In terms of imputation, future
339 improved models can become practically very useful, largely for GWAS studies in
340 which imputation is a common application to increase resolution. Different generative
341 models such as MaskGAN (Fedus et al. 2018) which demonstrated good results in text
342 gap filling might also be adapted for genetic imputation. RBM is possibly another option
343 to be used as an imputation tool directly by itself, since once the weights have been
344 learned, it is possible to fix a subset of the visible variables and to compute the average
345 values of the unobserved ones by sampling the probability distribution (in fact, it is
346 even easier than sampling entirely new configurations since the fixed subset of
347 variables will accelerate the convergence of the sampling algorithm).

348

349 Scans for detecting selection are another promising use case for AGs. The XP-EHH
350 and PBS scores computed on AGs were highly correlated with the scores of real
351 genomes. In particular, the highest peak we obtained for Estonian genomes was also
352 present in AGs, although it was the second highest peak in RBM XP-EHH plot (Figure
353 4). This peak falls within the range of skin color associated *SLC24A5* gene, which is
354 potentially under positive selection in many European populations (Basu Mallick et al.
355 2013).

356

357 As an additional feature, training an RBM to model the data distribution gives access
358 to a latent encoding of data points, providing a potentially easier to use representation
359 of data (Supplementary Figure 5). Future works could augment our current GAN model
360 to also provide an encoding mechanism, in the spirit of (Dumoulin et al. 2016 Jun 2),
361 (Chen et al. 2016) or (Donahue et al. 2016). These interpretable representations of the
362 data are expected to be more relevant for downstream tasks (Chen et al. 2016) and
363 could be used as a starting point for various population genetics analyses such as
364 demographic and selection inference, or yet unknown tasks.

365

366 Although there are some current limitations, generative models will most likely become
367 prominent for genetics in the near future with many promising applications. In this work,
368 we demonstrated the first possible implementations and use of AGs in the forthcoming
369 field which we would like to name artificial genomics.

370 **Materials & Methods**

371 **Data:**

372 We used 2504 individual genomes from 1000 Genomes Project (1000 Genomes
373 Project Consortium 2015) and 1000 individuals from Estonian Biobank (Leitsalu et al.
374 2015) to create artificial genomes (AGs). Additional 2000 Estonians were used as a
375 test dataset. Another Estonian dataset consisting of 8678 individuals which were not
376 used in training were used for imputation. Analyses were applied to a highly
377 differentiated 805 SNPs selected as a subset from (Colonna et al. 2014), 3348 SNPs
378 dispersed over the whole chromosome 15 and a dense 10000 SNP range/region from
379 chromosome 15. We also used a narrowed down version of the same region from
380 chromosome 15 with 5000 SNPs with an additional eye color column for unphased
381 genotype data using another 1925 Estonians as training dataset. In this set, 958 of the
382 Estonian samples have brown (encoded as 1) and 967 have blue eyes (encoded as
383 0). In the data format we used, rows are individuals/haplotypes (instances) and
384 columns are positions/SNPs (features). Each allele at each position is represented
385 either by 0 or 1. In the case of phased data (haplotypes), each column is one position
386 whereas in the case of unphased data, each two column corresponds to a single
387 position with alleles from two chromosomes.

388

389 **GAN Model:**

390 We used python-3.6, Keras 2.2.4 deep learning library with TensorFlow backend
391 (Chollet 2015), pandas 0.23.4 (McKinney 2010) and numpy 1.16.4 (Oliphant 2007) for
392 the GAN code. Generator of the GAN model we present consists of an input layer with
393 the size of the latent vector size 600, one hidden layer with size proportional to the
394 number of SNPs as $\text{SNP_number}/1.2$ rounded, another hidden layer with size
395 proportional to the number of SNPs as $\text{SNP_number}/1.1$ rounded and an output layer
396 with the size of the number of SNPs. The latent vector was set with
397 `numpy.random.normal` function setting the mean of the distribution as 0 and the
398 standard deviation as 1. The discriminator consists of an input layer with the size of
399 the number of SNPs, one hidden layer with size proportional to the number of SNPs
400 as $\text{SNP_number}/2$ rounded, another hidden layer with size proportional to the number
401 of SNPs as $\text{SNP_number}/3$ rounded and an output layer of size 1. All layer outputs
402 except for output layers have LeakyReLU activation functions with leaky_alpha

403 parameter 0.01 and L2 regularization parameter 0.0001. The generator output layer
404 activation function is tanh and discriminator output layer activation function is sigmoid.
405 Both discriminator and combined GAN were compiled with Adam optimization
406 algorithm with binary cross entropy loss function. We set the discriminator learning rate
407 as 0.0008 and combined GAN learning rate as 0.0001. For 5000 SNP data, the
408 discriminator learning rate was 0.00008 and combined GAN learning rate was 0.00001.
409 Training to test dataset ratio was 3:1. We used batch size of 32 and trained all datasets
410 up to 20000 epochs. We tried stopping the training based on AA_{TS} scores. The score
411 was calculated at 200 epoch intervals. For 805 SNP data, AA_{TS} converged very quickly
412 close to optimum 0.5 score. However, the difference between AA_{truth} and AA_{syn} scores
413 indicates possible overfitting to multiple data points so it was difficult to define a
414 stopping point. For 10K SNP data, convergence was observed after ~30K epochs (to
415 around 0.75) and reduced the number of fixed alleles in AGs but the gain was very
416 minimal (Supplementary Figure 16). Additionally, GAN was prone to mode collapse
417 especially after 20K epochs which resulted in multiple failed training attempts.
418 Therefore, we stopped training based on coherent PCA results of AGs with real
419 genomes. During each batch in the training, when only the discriminator is trained, we
420 applied smoothing to the real labels (1) by vectoral addition of random uniform
421 distribution via numpy.random.uniform with lower bound 0 and upper bound 0.1.
422 Elements of the generated outputs were rounded to 0 or 1 with numpy.rint function.
423

424 **RBM Model:**

425 The RBM was coded in Julia (Bezanson et al. 2017), and all the algorithm for the
426 training has been done by the authors. The part of the algorithm involving linear algebra
427 used the standard package provided by Julia. Two versions of the RBM were
428 considered. In both versions, the visible nodes were encoded using Bernoulli random
429 variables {0,1}, and the size of the visible layer was the same size as the considered
430 input. Two different types of hidden layers were considered. First with a sigmoid
431 activation function (hence having discrete {0,1} hidden variables), second with ReLu
432 (Rectified Linear unit) activations in which case the hidden variables were positive and
433 continuous (there are distributed according to a truncated gaussian distribution when
434 conditioning on the values of the visible variables). Results with sigmoid activation
435 function were worse compared to ReLu so we used ReLu for all the analyses
436 (Supplementary Figure 17MY). The number of hidden nodes considered for the

437 experiment was $N_h=100$ for the 805 SNP dataset and $N_h=500$ for the 10k one. There
438 is no canonical way of fixing the number of hidden nodes, in practice we checked that
439 the number of eigenvalues learnt by the model was smaller than the number of hidden
440 nodes, and that by adding more hidden nodes no improvement were observed during
441 the learning. The learning in general is quite stable, in order to have a smooth learning
442 curve, the learning rate was set between 0.001 and 0.0001 and we used batch size of
443 32. The negative term of the gradient of the likelihood function was approximated using
444 the PCDk method (Brügge et al. 2013), with $k=10$ and 100 of persistent chains. As a
445 stopping criterion, we looked at when the AA_{TS} score converges to the ideal value of
446 0.5 when sampling the learned distribution. When dealing with large and sparse
447 datasets for selection tests, RBM model did not manage to provide reasonable AA_{TS}
448 scores because the sampling is intrinsically difficult for large systems with strong
449 correlation. In that case, we used coherent PCA results as a stopping criterion.

450

451 **Bernoulli Distribution Model:**

452 We used python-3.6, pandas 0.23.4 and numpy 1.16.4 for the Bernoulli distribution
453 model code. Each allele at a given position was randomly drawn given the derived
454 allele frequency in the real population.

455

456 **Markov Chain Model:**

457 We used python-3.6, pandas 0.23.4 and numpy 1.16.4 for the Markov chain model
458 code. Allele at the initial position was set by drawing from a Bernoulli distribution
459 parameterized with the real frequency. Each successive allele was then drawn
460 randomly according to its probability given the previous sequence window. After the
461 initial position, the sequence window size increased incrementally up to a predefined
462 window size (5 or 10 SNPs).

463

464 **Chromosome Painting:**

465 We compared the haplotype sharing distribution between real and artificial
466 chromosomes through ChromoPainter (Lawson et al. 2012). In detail, we have painted
467 100 randomly selected “real” and “artificial” Estonians (recipients) against all the 1000
468 Genome Project phased data (donors). The nuisance parameters -n (348.57) and -M
469 (0.00027), were estimated running 10 iterations of the expectation-maximization
470 algorithm on a subset of 3,800 donor haplotypes.

471

472 **Haplostrips:**

473 We used Haplostrips (Marnetto and Huerta-Sánchez 2017) to visualize the haplotype
474 structure of real and artificial genomes. We extracted 500 individuals from each sample
475 set (Real, GAN AGs, RBM AGs) and considered them as different populations. Black
476 dots represent derived alleles, white dots represent ancestral alleles. The plotted SNPs
477 were filtered for a population specific minor allele frequency >5%; haplotypes were
478 clustered and sorted for distance against the consensus haplotype from the real set.
479 See the application article for further details about the method.

480

481 **Nearest Neighbour Adversarial Accuracy (AA_{TS}) and Privacy Loss**

482 We used the following equations for calculating AA_{TS} and privacy loss scores (Yale et
483 al. 2019):

484
$$AA_{truth} = \frac{1}{n} \sum_{i=1}^n \mathbf{1}(d_{TS}(i) > d_{TT}(i))$$

485
$$AA_{syn} = \frac{1}{n} \sum_{i=1}^n \mathbf{1}(d_{ST}(i) > d_{SS}(i))$$

486
$$AA_{TS} = \frac{1}{2}(AA_{true} + AA_{syn})$$

487
$$Privacy\ Loss = Test\ AA_{TS} - Train\ AA_{TS}$$

488

489 where n is the number of real samples as well as of artificial samples; $\mathbf{1}$ is a function
490 which takes the value 1 if the argument is true and 0 if the argument is false; $d_{TS}(i)$ is
491 the distance between the real genome indexed by i and its nearest neighbour in the
492 artificial genome dataset; $d_{ST}(i)$ is the distance between the artificial genome indexed
493 by i and its nearest neighbour in the real genome dataset; $d_{TT}(i)$ is the distance of the
494 real genome indexed by i to its nearest neighbour in the real genome dataset; $d_{SS}(i)$
495 is the distance of the artificial genome indexed by i to its nearest neighbour in the
496 artificial genome dataset. An AA_{TS} score of 0.5 is optimal whereas lower values
497 indicate overfitting and higher values indicate underfitting. For a better resolution for
498 the detection of overfitting, we also provided AA_{truth} and AA_{syn} metrics identified in the
499 general equation of AA_{TS} . If $AA_{TS} \approx 0.5$ but $AA_{truth} \approx 0$ and $AA_{syn} \approx 1$, this means that
500 the model is not overfitting in terms of a single data point but multiple ones. In other

501 words, the model might be focusing on small batches of similar real genomes to create
502 artificial genomes clustered at the center of each batch.

503

504 **Selection Tests:**

505 We used scikit-allel package for XP-EHH (Sabeti et al. 2007) and PBS (Yi et al. 2010)
506 tests. We used 1000 Estonian individuals (2000 haplotypes) with 3348 SNPs which
507 were homogenously dispersed over chromosome 15 for the training of GAN and RBM
508 models. For XP-EHH, Yoruban (YRI, 216 haplotypes) population from 1000 Genomes
509 data was used as the complementary population. For PBS, Yoruban (YRI, 216
510 haplotypes) and Japanese (JPT, 208 haplotypes) populations from 1000 Genomes
511 data were used as complementary populations. PBS window size was 10 and step
512 size was 5, resulting in 668 windows. 216 real and 216 AG haplotypes were compared
513 for the analyses.

514 **Acknowledgements**

515 This work was supported by the European Union through the European Regional
516 Development Fund (Project No. 2014-2020.4.01.16-0024, MOBTT53: LP, DM, BY;
517 Project No. 2014-2020.4.01.16-0030: LO, FM); the Estonian Research Council grant
518 PUT (PRG243): LP; Laboratoire de Recherche en Informatique: FJ. Thanks to Inria
519 TAU team for providing computational resources. Thanks to Adrien Pavao for his
520 valuable insight into AA_{TS} score.

521 **References**

- 522
523 1000 Genomes Project Consortium, Auton A, Brooks LD, Durbin RM, Garrison EP,
524 Kang HM, Korbel JO, Marchini JL, McCarthy S, McVean GA, et al. 2015. A global
525 reference for human genetic variation. *Nature*. 526(7571):68–74.
526 doi:10.1038/nature15393.
- 527 Adrión JR, Galloway JG, Kern AD. 2019. Inferring the landscape of recombination
528 using recurrent neural networks. *bioRxiv*. doi:10.1101/662247.
- 529 Arjovsky M, Chintala S, Bottou L. 2017. Wasserstein generative adversarial
530 networks. In: 34th International Conference on Machine Learning, ICML 2017.
- 531 Basu Mallick C, Iliescu FM, Möls M, Hill S, Tamang R, Chaubey G, Goto R, Ho SYW,
532 Gallego Romero I, Crivellaro F, et al. 2013. The Light Skin Allele of SLC24A5 in
533 South Asians and Europeans Shares Identity by Descent. *PLoS Genet*. 9(11).
534 doi:10.1371/journal.pgen.1003912.
- 535 Bezanson J, Edelman A, Karpinski S, Shah VB. 2017. Julia: A fresh approach to
536 numerical computing. *SIAM Rev*. doi:10.1137/141000671.
- 537 Brock A, Donahue J, Simonyan K. 2018 Sep 28. Large Scale GAN Training for High
538 Fidelity Natural Image Synthesis. [accessed 2019 Aug 26].
539 <http://arxiv.org/abs/1809.11096>.
- 540 Cann HM. 2002. A Human Genome Diversity Cell Line Panel. *Science* (80-).
541 doi:10.1126/science.296.5566.261b.
- 542 Chen X, Duan Y, Houthooft R, Schulman J, Sutskever I, Abbeel P. 2016. InfoGAN:
543 Interpretable representation learning by information maximizing generative
544 adversarial nets. In: *Advances in Neural Information Processing Systems*.
- 545 Chollet F. 2015. Keras: Deep Learning library for Theano and TensorFlow. GitHub
546 Repos.
- 547 Colonna V, Ayub Q, Chen Y, Pagani L, Luisi P, Pybus M, Garrison E, Xue Y, Tyler-
548 Smith C, Abecasis GR, et al. 2014. Human genomic regions with exceptionally high
549 levels of population differentiation identified from 911 whole-genome sequences.
550 *Genome Biol*. doi:10.1186/gb-2014-15-6-r88.
- 551 Davidsen K, Olson BJ, DeWitt WS, Feng J, Harkins E, Bradley P, Matsen FA. 2019.
552 Deep generative models for T cell receptor protein sequences. *Elife*. 8.
553 doi:10.7554/elife.46935. [accessed 2019 Sep 12].
554 <https://elifesciences.org/articles/46935>.
- 555 Diaz-Papkovich A, Anderson-Trocme L, Gravel S. 2019. Revealing multi-scale
556 population structure in large cohorts. *bioRxiv*. doi:10.1101/423632.
- 557 Donahue J, Krähenbühl P, Darrell T. 2016 May 31. Adversarial Feature Learning.
558 [accessed 2019 Aug 28]. <http://arxiv.org/abs/1605.09782>.
- 559 Dumoulin V, Belghazi I, Poole B, Mastropietro O, Lamb A, Arjovsky M, Courville A.
560 2016 Jun 2. Adversarially Learned Inference. [accessed 2019 Aug 28].
561 <http://arxiv.org/abs/1606.00704>.
- 562 Dwork C, McSherry F, Nissim K, Smith A. 2006. Calibrating noise to sensitivity in
563 private data analysis. In: *Lecture Notes in Computer Science* (including subseries
564 *Lecture Notes in Artificial Intelligence* and *Lecture Notes in Bioinformatics*).
- 565 Eriksson N, Macpherson JM, Tung JY, Hon LS, Naughton B, Saxonov S, Avey L,

- 566 Wojcicki A, Pe'er I, Mountain J. 2010. Web-based, participant-driven studies yield
567 novel genetic associations for common traits. PLoS Genet.
568 doi:10.1371/journal.pgen.1000993.
- 569 Fedus W, Goodfellow I, Dai AM. 2018 Jan 23. MaskGAN: Better Text Generation via
570 Filling in the _____. [accessed 2019 Aug 26]. <http://arxiv.org/abs/1801.07736>.
- 571 Flagel L, Brandvain Y, Schrider DR. 2019. The unreasonable effectiveness of
572 convolutional neural networks in population genetic inference. Mol Biol Evol.
573 doi:10.1093/molbev/msy224.
- 574 Goodfellow I, Pouget-Abadie J, Mirza M. 2014. Generative Adversarial Networks
575 (GANs) - Tutorial. Neural Inf Process Syst.
- 576 Gurdasani D, Carstensen T, Tekola-Ayele F, Pagani L, Tachmazidou I, Hatzikotoulas
577 K, Karthikeyan S, Iles L, Pollard MO, Choudhury A, et al. 2015. The African Genome
578 Variation Project shapes medical genetics in Africa. Nature.
579 doi:10.1038/nature13997.
- 580 Han J, Kraft P, Nan H, Guo Q, Chen C, Qureshi A, Hankinson SE, Hu FB, Duffy DL,
581 Zhen ZZ, et al. 2008. A genome-wide association study identifies novel alleles
582 associated with hair color and skin pigmentation. PLoS Genet.
583 doi:10.1371/journal.pgen.1000074.
- 584 Hinton GE. 2007. Learning multiple layers of representation. Trends Cogn Sci.
585 doi:10.1016/j.tics.2007.09.004.
- 586 Hinton GE, Salakhutdinov RR. 2006. Reducing the dimensionality of data with neural
587 networks. Science (80-). doi:10.1126/science.1127647.
- 588 Howie B, Marchini J, Stephens M. 2011. Genotype imputation with thousands of
589 genomes. G3 Genes, Genomes, Genet. doi:10.1534/g3.111.001198.
- 590 Killoran N, Lee LJ, Delong A, Duvenaud D, Frey BJ. 2017 Dec 17. Generating and
591 designing DNA with deep generative models. [accessed 2019 Sep 15].
592 <http://arxiv.org/abs/1712.06148>.
- 593 Kingma DP, Welling M. 2013 Dec 20. Auto-Encoding Variational Bayes. [accessed
594 2019 Aug 26]. <http://arxiv.org/abs/1312.6114>.
- 595 Larochelle H, Bengio Y. 2008. Classification using discriminative restricted boltzmann
596 machines. In: Proceedings of the 25th International Conference on Machine
597 Learning.
- 598 Lawson DJ, Hellenthal G, Myers S, Falush D. 2012. Inference of population structure
599 using dense haplotype data. PLoS Genet. 8(1):11–17.
600 doi:10.1371/journal.pgen.1002453.
- 601 Ledig C, Theis L, Huszár F, Caballero J, Cunningham A, Acosta A, Aitken A, Tejani
602 A, Totz J, Wang Z, et al. 2017. Photo-realistic single image super-resolution using a
603 generative adversarial network. In: Proceedings - 30th IEEE Conference on
604 Computer Vision and Pattern Recognition, CVPR 2017.
- 605 Leitsalu L, Haller T, Esko T, Tammesoo ML, Alavere H, Snieder H, Perola M, Ng PC,
606 Mägi R, Milani L, et al. 2015. Cohort profile: Estonian biobank of the Estonian
607 genome center, university of Tartu. Int J Epidemiol. doi:10.1093/ije/dyt268.
- 608 Libbrecht MW, Noble WS. 2015. Machine learning applications in genetics and
609 genomics. Nat Rev Genet. doi:10.1038/nrg3920.

- 610 Liu Q, Lv H, Jiang R. 2019. HicGAN infers super resolution Hi-C data with generative
611 adversarial networks. In: Bioinformatics. Vol. 35. Oxford University Press. p. i99–
612 i107.
- 613 Lucas T, Tallec C, Verbeek J, Ollivier Y. 2018. Mixed batches and symmetric
614 discriminators for GAN training. In: 35th International Conference on Machine
615 Learning, ICML 2018.
- 616 Mallick S, Li H, Lipson M, Mathieson I, Gymrek M, Racimo F, Zhao M, Chennagiri N,
617 Nordenfelt S, Tandon A, et al. 2016. The Simons Genome Diversity Project: 300
618 genomes from 142 diverse populations. *Nature*. doi:10.1038/nature18964.
- 619 Mardis ER. 2017. DNA sequencing technologies: 2006–2016. *Nat Protoc*.
620 doi:10.1038/nprot.2016.182.
- 621 Marnetto D, Huerta-Sánchez E. 2017. Haplostrips: revealing population structure
622 through haplotype visualization. *Methods Ecol Evol*. 8(10):1389–1392.
623 doi:10.1111/2041-210X.12747.
- 624 McKinney W. 2010. Data Structures for Statistical Computing in Python. In:
625 Proceedings of the 9th Python in Science Conference.
- 626 Mitt M, Kals M, Pärn K, Gabriel SB, Lander ES, Palotie A, Ripatti S, Morris AP,
627 Metspalu A, Esko T, et al. 2017. Improved imputation accuracy of rare and low-
628 frequency variants using population-specific high-coverage WGS-based imputation
629 reference panel. *Eur J Hum Genet*. doi:10.1038/ejhg.2017.51.
- 630 Oliphant TE. 2007. SciPy: Open source scientific tools for Python. *Comput Sci Eng*.
- 631 Popejoy AB, Fullerton SM. 2016. Genomics is failing on diversity. *Nature*.
632 doi:10.1038/538161a.
- 633 Radford A, Metz L, Chintala S. 2016. Unsupervised Representation learning with
634 Deep Convolutional GANs. *Int Conf Learn Represent*. doi:10.1051/0004-
635 6361/201527329.
- 636 Rolnick D, Dyer EL. 2019. Generative models and abstractions for large-scale
637 neuroanatomy datasets. *Curr Opin Neurobiol*. doi:10.1016/j.conb.2019.02.005.
- 638 Sabeti PC, Varilly P, Fry B, Lohmueller J, Hostetter E, Cotsapas C, Xie X, Byrne EH,
639 McCarroll SA, Gaudet R, et al. 2007. Genome-wide detection and characterization of
640 positive selection in human populations. *Nature*. doi:10.1038/nature06250.
- 641 Salimans T, Goodfellow I, Zaremba W, Cheung V, Radford A, Chen X. 2016.
642 Improved techniques for training GANs. In: Advances in Neural Information
643 Processing Systems.
- 644 Sheehan S, Song YS. 2016. Deep Learning for Population Genetic Inference. *PLoS*
645 *Comput Biol*. 12(3):1–28. doi:10.1371/journal.pcbi.1004845.
- 646 Shimagaki K, Weigt M. 2019 Sep 5. Selection of sequence motifs and generative
647 Hopfield-Potts models for protein families. *bioRxiv*.:652784. doi:10.1101/652784.
- 648 Sirugo G, Williams SM, Tishkoff SA. 2019. The Missing Diversity in Human Genetic
649 Studies. *Cell*. doi:10.1016/j.cell.2019.02.048.
- 650 Smolensky P. 1986. Information processing in dynamical systems: Foundations of
651 harmony theory. In: Parallel Distributed Processing Explorations in the Microstructure
652 of Cognition.
- 653 Teh YW, Hinton GE. 2001. Rate-coded restricted boltzmann machines for face

- 654 recognition. In: Advances in Neural Information Processing Systems.
- 655 Torkzadehmahani R, Kairouz P, Ai G, Paten B. 2019. DP-CGAN : Differentially
656 Private Synthetic Data and Label Generation. Proceedings of the IEEE Conference
657 on Computer Vision and Pattern Recognition Workshops.
- 658 Tubiana J, Cocco S, Monasson R. 2019. Learning protein constitutive motifs from
659 sequence data. *Elife*. doi:10.7554/eLife.39397.
- 660 Yale A, Dash S, Dutta R, Guyon I, Pavao A, Bennett K. 2019 Apr 24. Privacy
661 Preserving Synthetic Health Data. [accessed 2019 Aug 27]. <https://hal.inria.fr/hal-02160496/>.
- 663 Yi X, Liang Y, Huerta-Sanchez E, Jin X, Cuo ZXP, Pool JE, Xu N, Jiang H,
664 Vinckenbosch N, Korneliussen TS, et al. 2010. Sequencing of 50 human exomes
665 reveals adaptation to high altitude. *Science* (80-). doi:10.1126/science.1190371.
- 666 Zhang H, Xu T, Li H, Zhang S, Wang X, Huang X, Metaxas D. 2017. StackGAN: Text
667 to Photo-Realistic Image Synthesis with Stacked Generative Adversarial Networks.
668 In: Proceedings of the IEEE International Conference on Computer Vision.
- 669 Zhang M, Song F, Liang L, Nan H, Zhang J, Liu H, Wang LE, Wei Q, Lee JE, Amos
670 CI, et al. 2013. Genome-wide association studies identify several new loci associated
671 with pigmentation traits and skin cancer risk in European Americans. *Hum Mol
Genet*. doi:10.1093/hmg/ddt142.
- 673